

Original Paper

Calbindin-D_{9k} is a Novel Risk Gene for Neurodegenerative Disease

Eui-Man Jung^a Yeong-Min Yoo^a Seon Young Park^a Changhwan Ahn^a
Bo-Hui Jeon^a Eui-Ju Hong^b Woo-Yang Kim^c Eui-Bae Jeung^a

^aLaboratory of Veterinary Biochemistry and Molecular Biology, Veterinary Medical Center and College of Veterinary Medicine, Chungbuk National University, Cheongju, Chungbuk, Republic of Korea, ^bCollege of Veterinary Medicine, Chungnam National University, Yuseong, Daejeon, Republic of Korea, ^cDepartment of Biological Sciences, Kent State University, Kent, OH, USA

Key Words

Calbindin-D_{9k} • Neurodegenerative diseases • Alzheimer's disease • Parkinson's disease

Abstract

Background/Aims: Calcium homeostasis plays a crucial role in neuronal development and disease. Calbindin-D_{9k} (CaBP-9k) acts as calcium modulators and sensors in various tissues. However, the neurobiological functions of CaBP-9k are unknown. **Methods:** We used CaBP-9k knockout (KO) mice to investigate the roles of these gene in neurodegenerative diseases, such as Alzheimer's and Parkinson's diseases. We used anatomical and biochemical approaches to characterize functional abnormalities of the brain in the CaBP-9k KO mice. **Results:** We found that the brains of CaBP-9k KO mice have increased APP/ β -amyloid, Tau, and α -synuclein accumulation and endoplasmic reticulum (ER) stress-induced apoptosis. Neurons deficient for these CaBP-9k had abnormal intracellular calcium levels and responses. ER stress inhibitor TUDCA reduced ER stress-induced apoptosis and restored ER stress- and apoptosis-related proteins expression to wild-type levels in CaBP-9k KO mice. Furthermore, treatment with TUDCA rescued the abnormal memory and motor behaviors exhibited by older CaBP-9k KO mice. **Conclusion:** Our results suggest that a loss of CaBP-9k may contribute to the onset and progression of neurodegenerative diseases.

© 2020 The Author(s). Published by
Cell Physiol Biochem Press GmbH&Co. KG

Introduction

Calcium is a ubiquitous second messenger stored intracellularly in mitochondria and in the endoplasmic reticulum (ER) [1] in a diversity of cell types, including neurons, in which it regulates various functions such as synaptic transmission, plasticity, and survival. Calcium homeostasis in neurons involves tight regulation of cytosolic concentrations, the disruption of which can lead to synaptic failure, network dysfunction, and cognitive impairment as

E.-M. Jung and Y.-M. Yoo have contributed equally to this work.

Prof. Eui-Bae Jeung

Laboratory of Veterinary Biochemistry and Molecular Biology, Veterinary Medical Center and College of Veterinary Medicine, Chungbuk National University, Cheongju, Chungbuk 28644 (Republic of Korea)
Tel. +82-43-261-2397, Fax +82-43-267-3150, E-Mail ebejeung@chungbuk.ac.kr

well as neuronal death and various neurodegenerative diseases [2, 3]. For example, altered calcium homeostasis in the ER is associated with the pathogenesis of Alzheimer's disease [3], as high intracellular concentrations induce amyloid precursor protein (APP)/ β -amyloid and Tau accumulation and neuronal cell death. Elevated calcium levels also disrupt mitochondrial and ER function contributing to the death of dopamine neurons in the substantia nigra pars compacta (SNc) that characterize Parkinson's disease [4].

The homeostasis of intracellular calcium concentrations involves the binding of cytosolic calcium to members of the EF-hand family of proteins, including calbindin-D_{9k} (CaBP-9k) and calbindin-D_{28k} (CaBP-28k) [5, 6]. CaBP-9k is widely distributed and this protein is co-expressed in mature-, GABAergic, dopaminergic, and oxytocinergic neurons in the rat brain [7]. Furthermore, CaBP-28k is widely distributed throughout the central nervous system, where it is found in the somas, axons, and terminals of neurons. CaBP-28k plays roles in the differentiation and plasticity of hippocampal neurons [8], and may protect neurons from elevated intracellular calcium levels in Alzheimer's disease [9, 10]. Its expression is decreased in temporal and parietal cortices of patients with dementia of other histopathological types [11]. CaBP-28k is also expressed in neurons of the SNc and ventral tegmental area (VTA) in rats and monkeys [12, 13], and CaBP-28k protects VTA dopamine neurons against oxidative stress, calcium toxicity, and α -synuclein accumulation in Parkinson's disease [14]. Less is known about CaBP-9k, which along with CaBP-28k, suppresses prion protein expression and may be influenced by prion disease in mouse brains [15, 16]. CaBP-9k expression induced by melatonin also suppresses hydrogen peroxide-mediated cell death in rat pituitary GH3 cells [17, 18].

To provide a clearer understating of the roles of these CaBP-9k in the brain, we used CaBP-9k knockout (KO) mice. We found that CaBP-9k KO leads to neurodegeneration resembling Alzheimer's and Parkinson's diseases, with increases in APP/ β -amyloid, Tau, and α -synuclein and ER stress-induced apoptosis in the brains of CaBP-9k KO mice. Furthermore, CaBP-9k ablation induced abnormal memory and motor behaviours, which were rescued by treatment with an ER stress inhibitor, tauroursodeoxycholic acid (TUDCA). The findings presented here establish a critical role for CaBP-9k in the pathogenesis of neurodegenerative diseases, such as Alzheimer's and Parkinson's diseases.

Materials and Methods

CaBP-9k knockout mice and TUDCA treatment

CaBP-9k KO mice were generated as previously described [19, 20]. The genotypes of offspring were determined by PCR analysis, as described previously [19]. The Mice were housed in a cage with 12:12h light-dark cycle. No more than 5 mice were housed in a cage. Mice were handled according to a protocol approved by the Ethics Committee of the Chungbuk National University. TUDCA-treated mice were fed a diet of standard laboratory chow (Purina Mills, USA) supplemented with either 0.4 % (wt/wt) TUDCA (sodium salt; Matrix Scientific, USA). Treatment was started when the mice were 5 months old and continued for 8 months. Behavioral testing started at 7 months of age, where CaBP-9k KO mice start to display memory deficits and lasted for a month. Weight was measured at the beginning of the treatment TUDCA and general activity was monitored during experiments.

Real-time reverse transcription PCR

Quantitative real-time PCR was performed as described previously [21]. Total RNA was extracted from wild-type and CaBP-9k mutant brains using Trizol reagent (Invitrogen). First-strand complementary DNA (cDNA) was prepared by reverse transcription using the MMLV cDNA synthesis kit (Thermo Fisher Scientific). To determine the conditions for the logarithmic phase during PCR amplification with target mRNA, aliquots (1 μ g) were amplified using different numbers of cycles. A linear relationship between PCR product band visibility and the number of amplification cycles was observed for target mRNAs. Real-time PCR was performed with 1 μ l of the cDNA template added to 10 μ l of 2x SYBR Premix Ex Taq (TaKaRa Bio) and specific primers (10 pM each). Primer sequences are presented in Supplementary Table 1 (for all

supplemental material see www.cellphysiolbiochem.com). Real-time PCR (Applied Biosystems) was carried out for 40 cycles of denaturation at 95°C for 15 sec, annealing at 60°C for 15 sec, and extension at 72°C for 15 sec. Target gene expression was quantified relative to that of an internal control gene (*Gapgh*) based on the comparison of the threshold cycle (CT) at constant fluorescence intensity. The amount of transcript was inversely related to the observed CT and the CT was expected to increase by 1 for every two-fold dilution of the transcript. Relative expression (R) was calculated using the equation $R = 2^{-[\Delta CT_{\text{sample}} - \Delta CT_{\text{control}}]}$. All data were normalized relative to *Gapgh* as well as to the respective controls.

Western blot analysis

Western blotting was performed as described previously [21, 22]. Brain lysates were extracted with RIPA buffer (Invitrogen). Proteins (40 µg/lane) were separated on 10~15% SDS-PAGE gel and transferred to an immobilon-P membrane (Millipore) by a Mini Trans-Blot Electrophoretic Transfer Cell (Bio-Rad Laboratories). The resulting blot was blocked in TBS (tris-buffered saline) containing 5% BSA for 60 minutes, then incubated with a primary antibody rabbit anti-calbindin- D_{9k} (Invitrogen, PA5-68289, 1:1000), rabbit anti-BACE (Cell Signaling Technology, #5606, 1:1000), rabbit anti-Tau (Cell Signaling Technology, #4019, 1:1000), p-SAPK/JNK (Cell Signaling Technology, #9251, 1:1000), mouse anti-Bax (Santa Cruz, sc-7480, 1:500), mouse anti-Bcl-2 (Santa Cruz, sc-7382, 1:500), rabbit anti-cleaved caspase-3 (Cell Signaling Technology, #9664, 1:1000), rabbit anti-cleaved caspase-9 (Cell Signaling Technology, #7237, 1:1000), PARP (Cell Signaling Technology, #9532, 1:1000), mouse anti-GADD153/CHOP (Cell Signaling Technology, #2895, 1:1000), rabbit anti-p-PERK (Cell Signaling Technology, #3179, 1:1000), rabbit anti-PERK (Cell Signaling Technology, #3192, 1:1000), rabbit anti-p-IRE1 α (Thermo Fisher Scientific, PA1-16927, 1:1000), rabbit anti-IRE1 α (Cell Signaling Technology, #3294, 1:1000), rabbit anti-p-eIF2 α (Cell Signaling Technology, #3597, 1:1000), rabbit anti-caspase-12 (Cell Signaling Technology, #2202, 1:1000) and GAPDH (Santa Cruz, sc-25778, 1:500) for overnight at 4°C. After washing in TBS containing 0.1% Tween 20, the membrane was incubated with an appropriate horseradish peroxidase-conjugated secondary antibody (1:2500, Cell Signaling Technology) for 1 hour at room temperature. After washing, the membrane was developed by using ECL Western-blotting reagents (Pierce Biotechnology). Immunoreactive proteins were visualized by exposure to Agfa CP-BU X-ray film (Agfa-Gevaert NV). Protein bands were visualized by image-scanning, and optical density was measured by using ImageJ analysis software 1.37 after the data were corrected by background subtraction

Immunostaining

Immunostaining of brain sections or dissociated cells was performed as described previously [19, 21, 22]. Primary antibodies used were mouse anti-APP/ β -Amyloid (Cell Signaling Technology, #2450, 1:500), mouse anti-Tau (Cell Signaling Technology, #4019, 1:300), rabbit anti-PARP (Cell Signaling Technology, #9532, 1:500), rabbit anti-cleaved caspase-3 (Cell Signaling Technology, #9664, 1:500), mouse anti-BrdU (BD Biosciences, #555627, 1:800), rabbit anti-Ki67 (Cell Signaling Technology, #9129, 1:500), mouse anti- α -synuclein (Cell Signaling Technology, #2647, 1:500), chicken anti-tyrosine hydroxylase (AVES, TYH, 1:800), chicken anti-GFP (Invitrogen, A10262, 1:800), rabbit anti-calbindin- D_{9k} (Invitrogen, PA5-68289, 1:800) antibodies. Appropriate secondary antibodies conjugated with Alexa dyes (Invitrogen) were used to detect primary antibodies. DAPI (Sigma-Aldrich) was used to stain nuclei.

Cell culture

For evaluation of CaBP-9k knockdown by shRNA constructs, Neuro2a cells maintained in DMEM/10% FBS were transiently transfected using Lipofectamine LTX (Invitrogen) according to the manufacturer's instructions. Transfections were allowed to proceed for 4–5 hours, and then cells were cultured in 10% FBS/DMEM for 24 hours.

The primary neuronal cells were isolated from E14.5–16.5 CaBP-9k KO mice. Meninges were removed, and primary neuronal cells were dissociated with trituration after trypsin/EDTA treatment. The cells were plated onto poly-D-lysine/laminin-coated coverslips and cultured in the medium containing Neurobasal medium (Invitrogen), 2 mM glutamine, 2% (v/v) B27 supplement (Invitrogen), 1% (v/v) N2 supplement (Invitrogen), and 50 U/mL penicillin/streptomycin (Invitrogen).

TUNEL assay

As described previously [19, 21], tissue sections and cell cultures were fixed with 4% PFA, and in situ detection of cells with DNA-strand breaks was performed using In Situ Cell Death Detection Kit (Roche Diagnostics) according to the manufacturer's instruction.

Measurement of intracellular calcium

The primary neuronal cells were plated in 96 well plates. DIV7 neuronal cells were incubated with calcium dye, Rhod-4 (Abcam), for 1h at 37°C. The plates were then placed into a Lionheart™ FX Automated Microscope (BioTek) for the calcium response to monitor cell fluorescence (Rhod-4: Excitation = 540 nm and Emission = 590 nm). Images were acquired using a 4x objective at a rate of 3 frames per second. In-line injectors were used to dispense 20 µL of glutamate (30 µM, Sigma-Aldrich) into the wells, and cells were imaged for an additional 60 seconds to monitor response.

Behavioral assays

All behavioral assays were done during the light cycle. Health conditions including weights, activity and feeding were checked prior to assays. We used male and female mice for most behavioral assays. All behavioral assays were done blind to genotypes with age-matched littermates of mice.

Novel object recognition test. As described previously [21], a test mouse was first habituated to an open field arena (60 × 60 cm) for 5 min. Following habituation, the test mouse was removed from the arena and two identical objects with size (10.5 × 4.5 × 2.5 cm) were placed in the opposite corners of the arena, 15 cm from the side walls. Then the test mouse was reintroduced into the center of the arena and allowed to explore the arena including the two novel objects for 10 min. After 6 h, one object was replaced with another novel object, which was of similar size but different shape and color than the previous object. The same test mouse was placed in the arena to explore the arena and the two objects. The movement of mice was recorded by a camera for 10 min and further analyzed by the video tracking EthoVision XT 14 software (Noldus).

Passive avoidance test. Mice were individually habituated to the lighted compartment before a test. During the training session, each mouse was placed into the lighted compartment and the latency to enter the dark compartment was recorded. When the mouse entered the dark compartment with all four paws, a foot shock (2 mA, 3 sec) was delivered. During retention session 24 h later, each mouse was placed into lighted compartment again and the latency to enter the dark compartment was recorded.

Morris water maze test. Mice were introduced into the perimeter of a circular water-filled tank 90 cm in diameter and 42 cm in depth with visual cues that were present on the tank walls as spatial references. The tank was divided into four equal quadrants (Q1-4) by lines drawn on the floor. A circular plexiglass platform was submerged 1 cm deep in Q2 and as such hidden from the mice. The mice started the task from one of three quadrants Q1, Q3 and Q4, varied by day of testing. Four trials were performed per mouse per day for ten days. Each trial lasted 1 minute and ended when the mouse climbed onto and remained on the hidden platform for ten seconds. The mouse was given 20 seconds to rest on the platform between trials. The time taken by the mouse to reach the platform was recorded as its latency. The time for four trials was averaged and recorded as a result for each mouse. On day 10, the mice were subjected to a single 60-second probe trial without a platform to test memory retention. The mice started the trial from Q4, the number of annulus crossings was counted, and the swimming path was recorded and analyzed using the Ethovision XT 14 tracking software (Noldus).

Cylinder test. Each mouse was placed in a transparent acrylic cylinder (10 cm in diameter and 14 cm high). The number of wall contacts with each forelimb when rearing in at least 15 rearing cycles was computed. Animals that did not meet this criterion were excluded from this assay. The cylinder test score was determined as follows: (use of the affected forepaw (contralateral) – intact forepaw (ipsilateral)/total (contralateral + ipsilateral + both).

Rotarod test. Using an accelerating rotarod apparatus (PanLab) the rotarod test was performed by placing mice on rotating drums (2.5 cm diameter) and measuring retention time on the rod. The speed of the rotarod accelerated from 4 to 40 rpm over a 5 min period. At least 20 min recovery time was allowed between trials.

Pole test. Mice were placed head-up on top of a metal pole (50 cm high and 1 cm wide) that has been wrapped in wooden wire. The base of the pole was placed in the home cage. When placed on the pole, mice

orient themselves downward and descend the length of the pole back into their home cage. The time to orient downward (t-turn) and the total time to descend (t-total) were measured.

Nesting behavior. Each animal was provided with a Nestlet (5 × 5 cm² piece of cotton; Ancare). After 24h, the next morning remaining Nestlets were scored on a scale from 1-5. (1) nesting material unmodified; (2) flat nest with partially shredded nesting material; (3) shallow nest with shredded material but lacking fully formed walls; (4) nest with well-developed walls; and (5) nest in a shape of a cocoon with a partial or complete roof. Pictures were taken of all nests.

Open field test. A mouse was placed near the wall-side of a 60 × 60 cm open-field arena, and the movement of the mouse was recorded by a camera for 5 min. The recorded video file was further analyzed using EthoVision XT 14 software (Noldus). The number of entries into and the overall time spent in the center of the arena (30 × 30 cm imaginary square) were measured.

Tail suspension test. A mouse was suspended from the hook of a tail suspension test box, 60 cm above the surface of a table using adhesive tape placed 1 cm away from the tip of the tail. After 1 min acclimatization, immobility duration was recorded by a camera for 5 min. Mice were considered immobile only when they hung passively and were completely motionless.

Statistical analysis

Normal distribution was tested using the Kolmogorov-Smirnov test and variance was compared. Unless otherwise stated, statistical significance was determined using two-tailed unpaired Student's t-tests for two population comparison followed by the Bonferroni's post hoc test for multiple comparisons. Data were analyzed using the GraphPad Prism and presented as means ± SEM. *P* values for each comparison were described in the legends or supplementary information section. To determine and confirm sample sizes (*n*), we performed a power analysis. The values for the power (1-β) and the type I error rate (α) were 0.8 and 0.05 (or 0.01), respectively. Each experiment in this study was performed blind and randomized. Mice were assigned randomly to the various experimental groups, and data were collected and processed randomly. The allocation, treatment, and handling of mice were the same across study groups. Control mice were selected from the same litter as the test group. The individuals conducting the experiments were blinded to group allocation and the allocation sequence. Exclusion criteria for mice were based on abnormal health conditions including weights below 15g at 6 weeks and noticeably reduced activity or feeding as used in previous studies [23, 24]. Statistical data and *n* numbers for all behavioral assays were described in the legends.

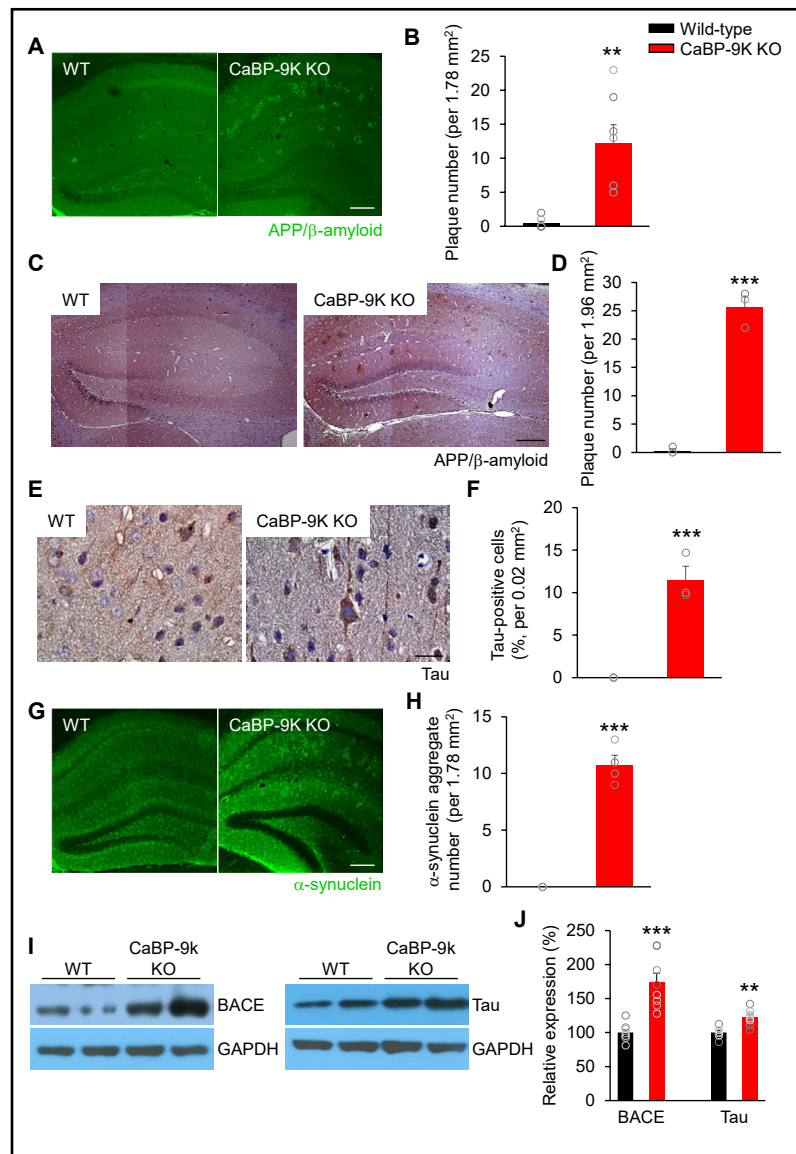
Results

Ablation of CaBP-9k induces signs indicative of Alzheimer's disease in mice

We first measured the expression of CaBP-9k in mouse brain extracts by Western blotting and real-time PCR. CaBP-9k mRNA and protein levels were undetectable in CaBP-9k KO mice. Moreover, CaBP-28k mRNA and protein levels in CaBP-9k KO mice were not different from those in wild-type mice (Supplementary Fig. 1). The localization of CaBP-9k was examined by immunostaining, which revealed a wide distribution of CaBP-9k-positive cells throughout the brain, including the olfactory bulb, cerebral cortex, hippocampus, thalamus, hypothalamus, paraventricular nucleus, SNc, VTA, cerebellum, and brain stem. Double immunostaining revealed that CaBP-9k was expressed by mature (NeuN-positive) and dopaminergic (tyrosine hydroxylase [TH]-positive) neurons in the hippocampus and in the SNc and VTA, respectively (Supplementary Fig. 2). Immunostaining for microtubule associated protein 2 (MAP2) revealed that CaBP-9k KO did not alter the lengths or numbers of primary and secondary neurites (Supplementary Fig. 3).

As an accumulation of APP/β-amyloid [25, 26], Tau protein [27, 28], and α-synuclein [29] in the hippocampus are hallmarks of Alzheimer's disease, we examined these proteins in CaBP-9k KO mice. Immunostaining for APP/β-amyloid revealed an increase in plaque numbers with age when comparing young (<2 months) and old (>8 months) CaBP-9k KO mice. Furthermore, the numbers of hippocampal plaques were significantly higher in CaBP-9k KO than in wild-type mice at an old age (Immunofluorescence: wild-type, 0.43 ± 0.32

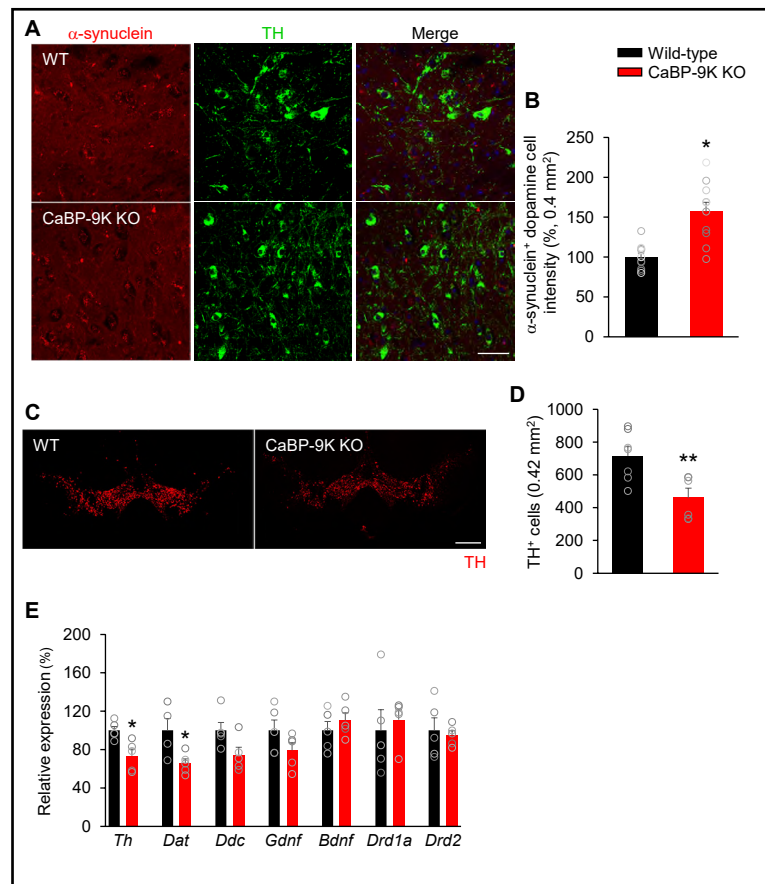
Fig. 1. CaBP-9k knockout causes Alzheimer's disease in mice. (A,C) Hippocampal sections of old wild-type (WT) and CaBP-9k KO mice were stained for APP/ β -amyloid by immunofluorescence and immunohistochemistry. Scale bar= 200 μ m. (B,D) Quantification of A and C. (Immunofluorescence: n = 7 mice for each group; Immunohistochemistry: n = 3 for mice for each group). (E) Immunohistochemistry for Tau in the hippocampi of old CaBP-9k KO mice. Scale bar= 20 μ m. (F) Quantification of E. n = 3 for mice for each group. (G) Immunofluorescence staining of α -synuclein aggregates in the hippocampi of old CaBP-9k KO mice. Scale bar= 200 μ m. (H) Quantification of G. n = 4 mice for each group. (I) Western blotting with antibodies to BACE and Tau using brain lysates from old wild-type and CaBP-9k KO mice. (J) Quantification of I. n = 8 for mice for each group. The intensities of the protein bands were normalized to the GAPDH



level. Data shown are the means \pm SEMs and were analysed by two-tailed unpaired Student's t-tests.

cells; CaBP-9k KO, 12.29 \pm 2.65 cells/1.78 mm²; Immunohistochemistry: wild-type, 0.33 \pm 0.33 cells; CaBP-9k KO, 25.67 \pm 1.86 cells/1.78 mm²) (Fig. 1A-D). In young mice, hippocampal APP/ β -amyloid plaques were undetectable in CaBP-9k KO mice (Supplementary Fig. 4A). Similarly, the densities of Tau-immunopositive neurons were significantly higher in CaBP-9k KO than in wild-type mice at an old age (CaBP-9k KO, 11.49 \pm 1.61 cells/0.02 mm²) (Fig. 1E, F). Additionally, the densities of hippocampal α -synuclein aggregates were increased in CaBP-9k KO at an old age (CaBP-9k KO, 10.75 \pm 0.85 cells/1.78 mm²) (Fig. 1G, H). In young mice, α -synuclein aggregate were undetectable in CaBP-9k KO mice (Supplementary Fig. 5A). The expression levels of beta-secretase (BACE) and another biomarker for Alzheimer's disease, Tau, were assessed by Western blotting. The levels of BACE and Tau were significantly increased in old CaBP-9k KO mice (relative expression for BACE: wild-type, 100 \pm 4.64%; CaBP-9k KO, 173.66 \pm 13.68%; for Tau: wild-type, 100 \pm 2.72%; CaBP-9k KO, 122.39 \pm 4.19%), compared with brain lysates from wild-type mice at an old age (Fig. 1I, J). These results suggest that ablation of CaBP-9k may contribute to the development of Alzheimer's disease.

Fig. 2. CaBP-9k knockout causes Parkinson's disease in mice. (A) Immunofluorescence staining for α -synuclein and TH in dopaminergic cells in the SNc and VTA of old CaBP-9k KO mice. Scale bar= 500 μ m. (B) Quantification of A. n = 7 mice for wild-type; n = 6 mice for CaBP-9k KO mice. (C) SNc and VTA sections from old CaBP-9k KO mice were immunostained with TH antibodies. Scale bar= 40 μ m. (D) Quantification of C. n = 10 for mice for each group. (E) mRNA levels of dopamine-related genes were assessed in brain lysates from old wild-type and CaBP-9k KO mice by real-time PCR. n = 5 for mice for each group. mRNA levels were normalized to the GAPDH level. Data shown are the means \pm SEMs and were analysed by two-tailed unpaired Student's t-tests.



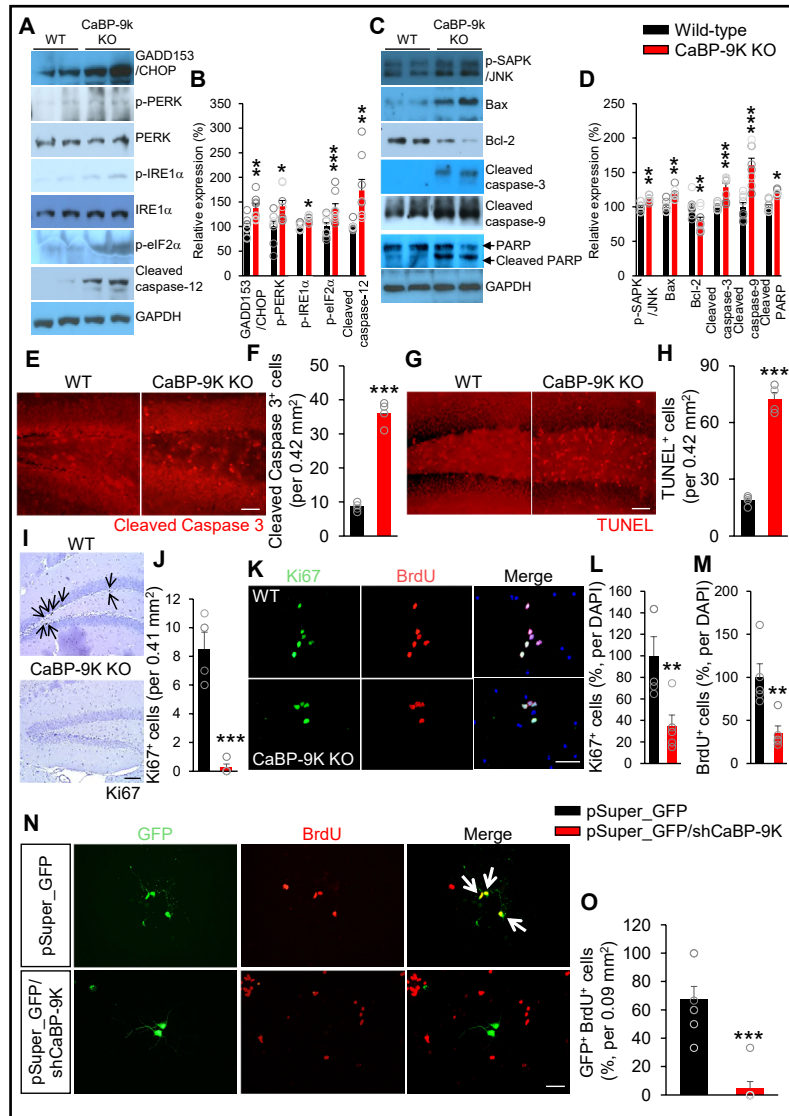
Ablation of CaBP-9k induces signs indicative of Parkinson's disease in mice

To determine if CaBP-9k KO results in a loss of dopaminergic cells in the SNc and VTA, which characterize Parkinson's disease [30, 31]. First, we assessed the intensity of α -synuclein immunofluorescence in TH-positive dopaminergic cells in SNc and VTA of young and old CaBP-9k KO mice and found increases of 56.65% in old CaBP-9k KO mice (relative intensity: wild-type, 100 \pm 5.13%; CaBP-9k KO, 156.65 \pm 12.11%) (Fig. 2A, B), and increases of 39.83% in young CaBP-9k KO mice (relative intensity: wild-type, 100 \pm 5.13%; CaBP-9k KO, 156.65 \pm 12.11%) (Supplementary Fig. 5B, C). Next, we examined TH immunostaining. We found that the numbers of TH-positive cells significantly decreased by 35.64% in CaBP-9k KO mice (wild-type, 715.71 \pm 56.86 cells; CaBP-9k KO, 460.67 \pm 58.55 cells/0.42 mm²), compared with that in the SNc and VTA of wild-type mice (Fig. 2C, D). Also, the decreases in the numbers of TH-positive cells suggest that the CaBP-9k KO mice may have abnormal expression of dopamine-related genes, such as those encoding *Th*, dopamine active transporter (*Dat*), dopadecarboxylase (*Ddc*), and glial cell line-derived neurotrophic factor (*Gdnf*). Real-time PCR analyses revealed that *Th* and *Dat* mRNA expression levels were decreased in the brains of CaBP-9k KO (relative expression for *Th*: wild-type, 100 \pm 4.09%; CaBP-9k KO, 73.55 \pm 6.96%; for *Dat*: wild-type, 100 \pm 12.38%; CaBP-9k KO, 65.61 \pm 4.78%). However, mRNA levels for genes encoding *Ddc*, *Gdnf*, brain-derived neurotrophic factor (*Bdnf*), dopamine receptor D1a (*Drd1a*) and dopamine receptor D2 (*Drd2*) were not altered by CaBP-9k KO (Fig. 2E). These results suggest that ablation of CaBP-9k may contribute to the development of Parkinson's disease.

Ablation of CaBP-9k induces loss of neurons by ER stress-induced apoptosis and suppressed proliferation

CaBP-9k act as intracellular calcium buffers and calcium sensors [32]. Therefore, the ablation of CaBP-9k may induce ER stress in neurons, resulting in apoptosis. We found that the protein levels of GADD153/CHOP and cleaved caspase-12 and the phosphorylation of PERK, IRE1 α and eIF2 α were significantly higher in brain lysates from old CaBP-9k KO than in those from wild-type mice (Fig. 3A, B). Levels of apoptosis markers, namely, Bax, cleaved caspase-3 and -9 and PARP, and SAPK/JNK phosphorylation, were significantly increased in brain lysates from CaBP-9k KO compared with in those from wild-type mice, whereas

Fig. 3. CaBP-9k knockout induces ER stress-induced apoptosis. (A) Western blotting with antibodies for ER stress-related proteins using brain lysates from old wild-type and CaBP-9k KO mice. (B) Quantification of A. n = 8 for mice for each group. The apoptosis markers were increased in old CaBP-9k KO mice. (C) Western blotting with antibodies for apoptosis-related proteins using brain lysates from old wild-type and CaBP-9k KO mice. (D) Quantification of C. n = 8 for mice for each group. The intensities of the protein bands were normalized to the GAPDH level. (E,G) Cell death was assessed in the hippocampi of old wild-type and CaBP-9k KO mice by immunostaining for cleaved caspase-3 or by TUNEL assays. Scale bar= 50 μ m. (F,H) Quantification of E and G. n = 4 for mice for each group. (I) Immunostaining of hippocampal sections from old CaBP-9k KO mice for the proliferation marker Ki67. Scale bar= 100 μ m. (J) Quantification of I. n = 4 for mice for each group. (K) Primary neuronal cells were cultured from embryonic day 13.5 wild-type and CaBP-9k KO mice for 2 days and then incubated with 100 μ M BrdU for 24 h before immunostaining for Ki67 and BrdU. Scale bar= 40 μ m. (L,M) Quantification of K. n = 5 cell culture replicates using 5 mice for each condition. (N) Primary neuronal cells cultured from embryonic day 12.5 wild-type and CaBP-9k KO mice for 3 days were transfected with pSuper_GFP/shCaBP-9k construct and then treated with BrdU for 24 h before immunostaining for GFP and BrdU. Scale bar= 40 μ m. (O) Quantification of N. n = 7 cell culture replicates using 7 mice for each condition. Data shown are the means \pm SEMs and were analysed by two-tailed unpaired Student's t-tests.



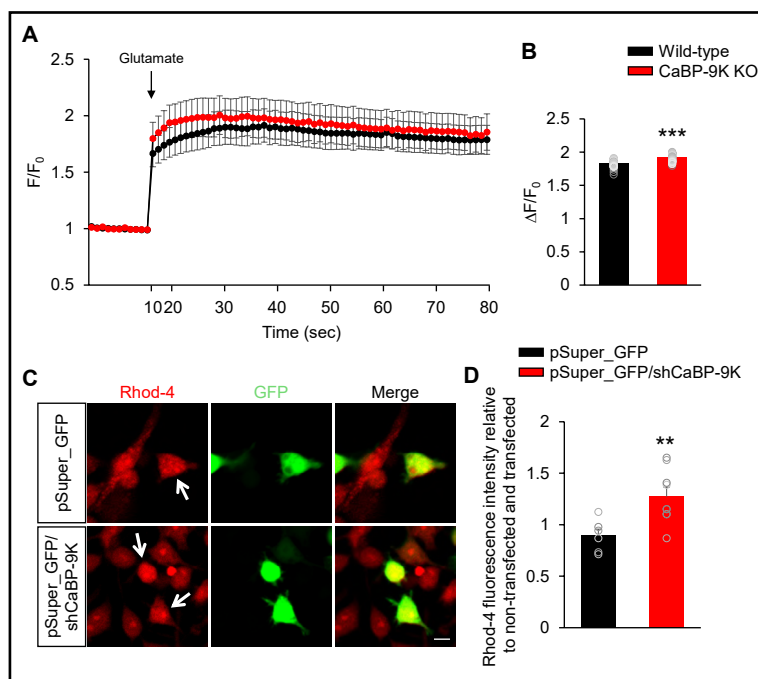
the levels of Bcl-2 were significantly decreased (Fig. 3C, D). Moreover, greater numbers of hippocampal cells immunopositive for cleaved caspase-3 were observed in young and old CaBP-9k KO mice than in their wild-type counterparts (young: wild-type, 6.67 ± 0.88 cells; CaBP-9k KO, 32.33 ± 1.76 cells/ 0.42 mm^2 ; old: wild-type, 8.50 ± 0.65 cells; CaBP-9k KO, 36.00 ± 1.78 cells/ 0.42 mm^2) (Fig. 3E, F and Supplementary Fig. 4B, C). Consistent with these results, TUNEL staining showed more cells with DNA fragmentation in young and old CaBP-9k KO than in their wild-type counterparts (young: wild-type, 12.00 ± 1.32 cells; CaBP-9k KO, 33.33 ± 2.08 cells/ 0.42 mm^2 ; old: wild-type, 18.75 ± 1.31 cells; CaBP-9k KO, 72.25 ± 3.68 cells/ 0.42 mm^2) (Fig. 3G, H and Supplementary Fig. 4D, E).

Next, we then examined the proliferation of neural progenitors in the dentate gyrus, which is the source of neurons in the adult brain. The numbers of Ki67-immunostained proliferating cells were significantly lower in old CaBP-9k KO than in the wild types (wild-type, 8.50 ± 1.19 cells; CaBP-9k KO, 0.25 ± 0.25 cells/ 0.41 mm^2) (Fig. 3I, J). In primary neuronal cultures, the percentages of Ki67- and BrdU-positive cells after a 24 h BrdU pulse were lower in cultures from CaBP-9k KO than in those from wild-type mice (% positive relative to wild-type for Ki67: wild-type, $100 \pm 17.93\%$; CaBP-9k KO, $34.53 \pm 10.54\%$; for BrdU: wild-type, $100 \pm 15.94\%$; CaBP-9k KO, $35.32 \pm 8.35\%$) (Fig. 3K-M). The effect of CaBP-9k ablation on neuronal proliferation was confirmed in cells transfected with pSuper_GFP/shCaBP-9k constructs (Supplementary Fig. 6). The numbers of proliferating shRNA-transfected cells (i.e., double-positive for GFP and BrdU) were reduced 92.91% for GFP/shCaBP-9k in comparison with control transfected cells (pSuper_GFP, $67.14 \pm 9.38\%$; pSuper_GFP/shCaBP-9k, $4.76 \pm 4.76\%$ / 0.09 mm^2) (Fig. 3N, O). Conclusion, these data show that the loss of CaBP-9k results in a loss of neurons from ER stress-induced apoptosis and reduced proliferation.

CaBP-9k ablation disrupts calcium levels

The loss of CaBP-9k in neurons may result in abnormal calcium responses and calcium levels. We assessed calcium influx in primary neuronal cultures from CaBP-9k knockout mouse via Rhod-4 staining. Peak calcium concentrations in response to glutamate treatment were significantly higher in neurons from CaBP-9k KO mice (Fig. 4A, B). However, the mRNA

Fig. 4. CaBP-9k knockout leads to abnormal calcium response and calcium levels. (A) Primary neuronal cells loaded with the calcium indicator Rhod-4 were monitored by a fluorometric imaging plate reader calcium assay. CaBP-9k KO neuronal cells were treated after 7 days in vitro with $50 \mu\text{M}$ glutamate (arrow). Traces represent mean values with the SEMs. (B) Histogram showing the distribution of the maximum observed amplitude compared with the baseline of each analysed cell. $n = 4$ experiments for each condition. (C) Intracellular calcium concentration in Neuro2a cells is measured by Rhod-4 loading. (D) Quantification of C. $n = 3$ cell culture replicates. Data shown are the means \pm SEMs and were analysed by two-tailed unpaired Student's t-tests.



levels of glutamate receptors were not different between wild-type and CaBP-9k KO brains (Supplementary Fig. 7D). Real-time PCR analyses revealed that transcript levels of calcium channel genes were mostly downregulated in the brains of old (Supplementary Fig. 7B), but not young (Supplementary Fig. 7A), CaBP-9k KO mice. These data suggest that CaBP-9k ablation impairs the regulation of intracellular calcium in neurons via abnormal calcium channel gene expression. We also found that knockdown of CaBP-9k induce an intracellular calcium concentration in Neuro2a cells (Fig. 4D, E). Conclusion, these results indicate that CaBP-9k are an important role in the regulation of intracellular calcium levels.

Abnormal memory and motor behaviour in CaBP-9k KO mice

We tested CaBP-9k KO mice for memory and motor behaviors that model clinical features of Alzheimer's and Parkinson's diseases [33]. In assessments of memory, old wild-type mice spent 19% more time approaching and remaining in the proximity of a novel object than the familiar object, whereas the CaBP-9k KO mice did not show any preference (Fig. 5A). However, the preference for a novel object was observed in young CaBP-9k KO mice (Supplementary Fig. 8A). In a passive avoidance conditioning test in old mice, the latency to enter a dark compartment was shorter for CaBP-9k KO mice than for wild-type mice (Fig. 5B), whereas there were no differences among young CaBP-9k KO mice (Supplementary

Fig. 5. CaBP-9k knockout mice show impaired memory and motor behavior. (A) Old wild-type and CaBP-9k KO mice were assessed in the novel object recognition test; the time spent exploring the objects is represented as a recognition index. n = 10 for mice for each group. (B) Old wild-type and CaBP-9k KO mice were assessed in the passive avoidance test; the latency to enter the dark compartment was recorded. n = 10 for mice for each group. (C) The Morris water maze assay reveals performance during training trials in old CaBP-9k KO and wild-type mice. (D) Representative swim paths of old mice during a probe trial after training. (E,F) Quantification of D. The old CaBP-9k KO mice exhibited decreased platform crossing numbers and escape latency. n = 12 for wild-type mice; n = 10 for CaBP-9k KO mice. (G) Contralateral forelimb use was assessed in old wild-type and CaBP-9k KO mice in the cylinder test. n = 6 for mice for each group. (H) The latency to fall was assessed in old mice in the rotarod test. n = 30 for mice for each group. (I) The turning time was assessed in old mice in the pole test. n = 10 for mice for each group. Data shown are the means ± SEMs and were analysed by two-tailed unpaired Student's t-tests.

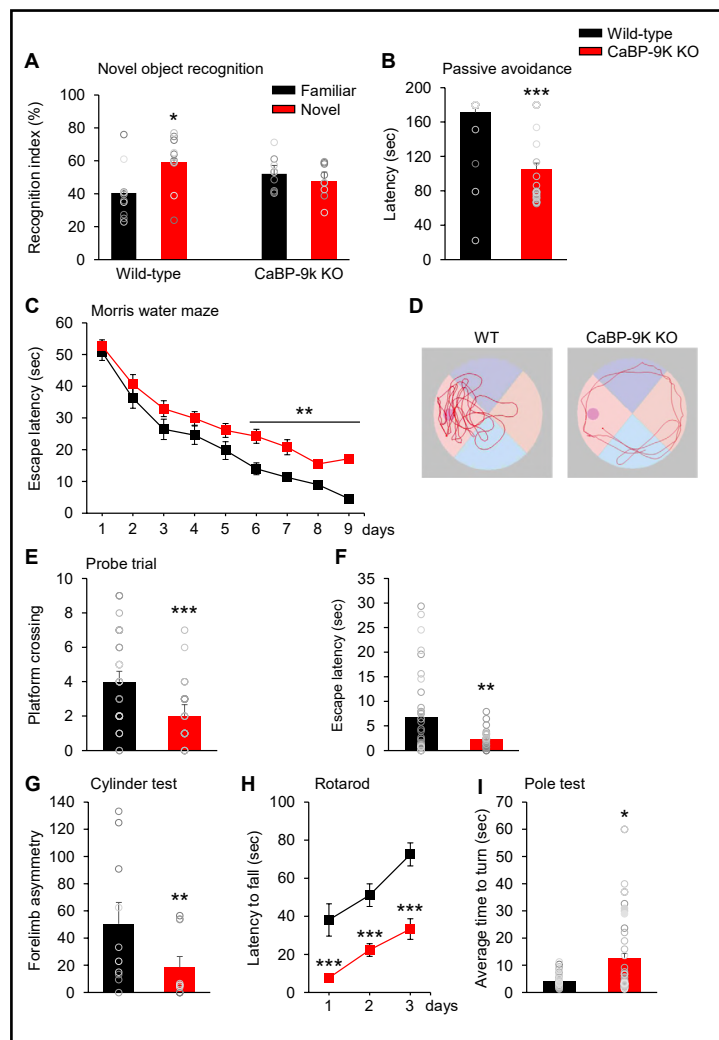


Fig. 8B). During the acquisition phase of the Morris water maze test, old CaBP-9k KO mice exhibited longer escape latencies than wild-type mice. A difference between CaBP-9k KO mice emerged after 6 days of training (Fig. 5C). Escape latencies among young CaBP-9k KO mice did not differ in the training process (Supplementary Fig. 8C). In probe trials of the Morris water maze test, old CaBP-9k KO mice crossed the platform fewer times than the wild-types (Fig. 5D-F), whereas young CaBP-9k KO were no differences (Supplementary Fig. 8D). In assessments of motor function using cylinder test, rotarod and pole test, old CaBP-9k KO mice showed significant impairments in contralateral forelimb use and motor learning and increased turning time on a pole, respectively (Fig. 5G-I), but no other motor impairments were observed in young CaBP-9k KO mice (Supplementary Fig. 8G-I). Additional testing was performed to assess other behaviours. For example, old CaBP-9k KO mice showed deficits in nest building, a social behaviour that provides shelter essential for heat conservation and reproduction, which was assessed 24 h after the nesting material was placed in their home cages (Supplementary Fig. 9C, D). However, this deficit was not displayed when young CaBP-9 KO mice were tested (Supplementary Fig. 9A, B). In the open field and tail suspension tests for the evaluation of anxiety and depression, respectively, no differences between young and old CaBP-9k KO and wild-type mice were observed (Supplementary Fig. 9G-J, M and N). Conclusion, these results demonstrate that CaBP-9k ablation produces memory and motor impairments in mice at an old age.

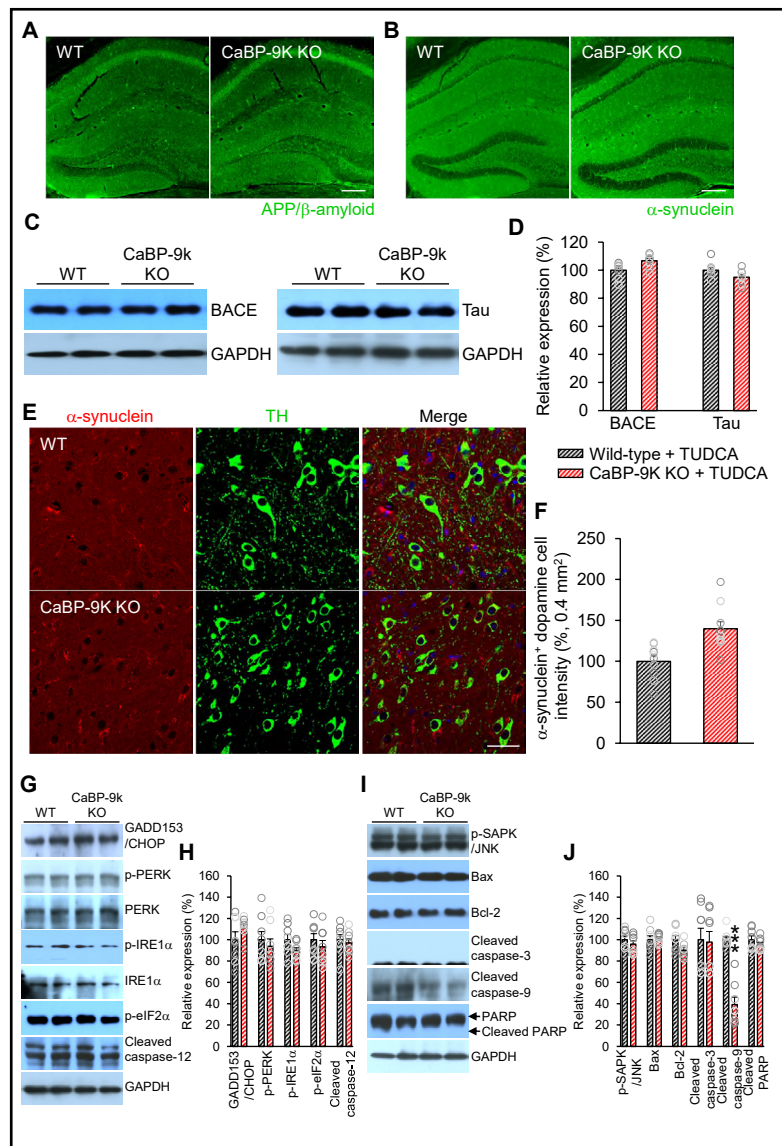
TUDCA reverses brain pathology in CaBP-9k KO mice

TUDCA is a pharmacological ER stress inhibitor that protects cells from ER stress-related apoptosis induced by abnormal calcium levels [34]. We fed presymptomatic 5 months CaBP-9k KO mice a diet of standard laboratory chow supplemented with 0.4% TUDCA for 3 months to determine if we could eliminate the brain pathologies induced by CaBP-9k ablation. First, we assessed the accumulation of APP/ β -amyloid and α -synuclein in the hippocampus. Interestingly, APP/ β -amyloid immunofluorescence was not detected in the hippocampi of TUDCA-treated CaBP-9k KO mice (Fig. 6A). Moreover, no α -synuclein staining was observed in any of the TUDCA-treated CaBP-9k KO mice (Fig. 6B). Protein levels of BACE and Tau did not differ between wild-type and CaBP-9k KO mice treated with TUDCA (Fig. 6C, D). Also, intensity of α -synuclein immunofluorescence in dopaminergic neurons in SNC and VTA did not differ between TUDCA-treated CaBP-9k KO and wild-type mice (Fig. 6E, F). Western blotting analyses revealed that treatment of CaBP-9k KO mice with TUDCA completely restored their expression of ER stress- and apoptosis-related proteins to wild-type levels, whereas the levels of cleaved caspase-9 were significantly decreased (Fig. 6K-N). Additionally, treatment with TUDCA restored or increased the expression of genes encoding calcium channels in CaBP-9k KO mice (Supplementary Fig. 7C). These data suggest that TUDCA suppresses ER stress and eliminates signs of pathology in the brains of CaBP-9k KO mice.

TUDCA rescues abnormal behaviors in CaBP-9k KO mice

We next examined whether TUDCA treatment can also rescue the abnormal behaviors observed in CaBP-9k KO mice. In the novel object recognition test, TUDCA-treated wild-type and CaBP-9k KO mice spent more time investigating the novel object than the familiar one (Fig. 7A). In the passive avoidance conditioning test, the latencies to enter the dark compartment were now similar among CaBP-9k KO mice (Fig. 7B). In addition, TUDCA treatment eliminated differences in escape latencies between wild-type and CaBP-9k KO mice in the Morris water maze test, such that the groups were not different after 6 days of training (Fig. 7C). CaBP-9k KO mice treated with TUDCA also performed as well as wild-type mice on the probe trials of the Morris water maze task, with no differences in the platform crossing times or escape latencies (Fig. 7D-F). With regard to motor behaviours, TUDCA treatment reversed the effects of CaBP-9k ablation on contralateral forelimb use and on motor learning in the rotarod test. In the pole test, CaBP-9k KO mice treated with TUDCA exhibited similar turning times (Fig. 7G-I). TUDCA treatment also improved the nesting behaviour in CaBP-9k

Fig. 6. TUDCA inhibits ER stress-induced apoptosis in CaBP-9k KO mice. (A) Immunofluorescence for APP/ β -amyloid plaques in hippocampi of old TUDCA-treated wild-type and CaBP-9k KO mice. Scale bar= 200 μ m. n = 4 mice for each group. (B) Immunofluorescence for α -synuclein in hippocampi of old TUDCA-treated wild-type and CaBP-9k KO mice. Scale bar= 200 μ m. (C) Western blotting for BACE and Tau expression in brain lysates from TUDCA-treated wild-type and CaBP-9k KO mice. (D) Quantification of C. n = 8 mice for each group. (E) Immunofluorescence staining for α -synuclein and TH in dopaminergic cells in the SNc and VTA in old TUDCA-treated wild-type and CaBP-9k KO mice. Scale bar= 40 μ m. (F) Quantification of E. n = 4 for mice for each group. (G,I) Western blotting for ER stress- and apoptosis-related proteins in old TUDCA-treated wild-type and CaBP-9k KO mice. (H,J) Quantification of G and I. n = 4 mice for each group. The intensities of the protein bands were normalized to the GAPDH level. Data shown are the means \pm SEMs and were analysed by two-tailed unpaired Student's t-tests.

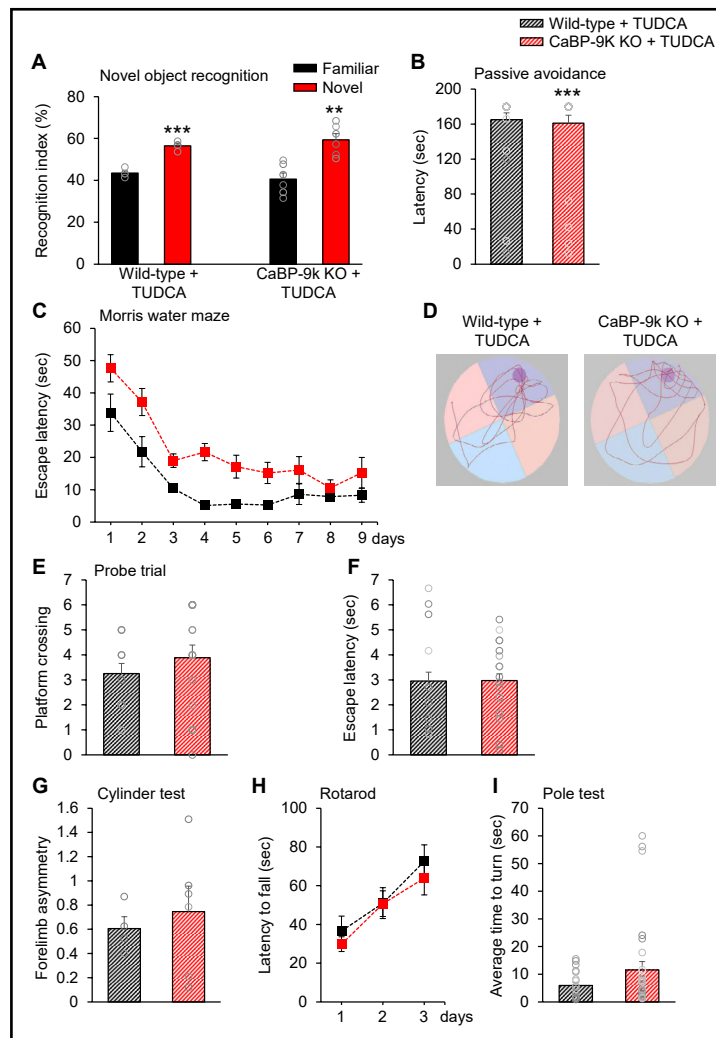


KO mice (Supplementary Fig. 9E, F), and no differences in the times spent in the centre area of an open field were seen among the mice (Supplementary Fig. 9K, L). Conclusion, these results show that TUDCA rescues impaired memory and motor behaviors in CaBP-9k KO mice.

Discussion

Calcium is involved in various developmental processes, such as cell differentiation, proliferation, and apoptosis [35-37] as well as neurotransmitter release and neuronal membrane excitability [38-40]. Essential factors for calcium homeostasis include CaBP-9k [41], which buffer increases in calcium levels [32], such as increases from 10^{-7} M in the resting cell to 10^{-5} M in the activated cell [42-44], and the ER, which regulates the uptake, storage, and mobilization of intracellular calcium [45]. Despite the link between altered calcium

Fig. 7. ER stress inhibitor rescues memory and motor behaviors in CaBP-9k KO mice. (A) Old TUDCA-treated wild-type and CaBP-9k KO mice were assessed in the novel object recognition test. (B) TUDCA-treated mice were assessed in the passive avoidance test. (C) In the Morris water maze test, escape latencies after 6 days of training were similar among TUDCA-treated mice. (D) Representative swim paths of TUDCA-treated wild-type and CaBP-9k KO mice during a probe trial after training. (E,F) Quantification of D. CaBP-9k KO mice treated with TUDCA showed no differences the platform crossing times or escape latency in probe trial. (G-I) Assessment of motor behaviors in the cylinder, rotarod, and pole tests. $n = 4$ for TUDCA-treated wild-type mice; $n = 6$ for TUDCA-treated CaBP-9k KO mice. Data shown are the means \pm SEMs and were analysed by two-tailed unpaired Student's t-tests.



homeostasis and neurodegenerative disease, the contributions by calcium-binding proteins are not well understood. Here, we report that CaBP-9k KO mice results in Alzheimer's and Parkinson's disease-like pathologies and that associated effects and behavioural impairments are rescued by the inhibition of ER stress, and this study will provide critical information regarding the pathogenic mechanisms of neurodegenerative diseases including Alzheimer's disease and Parkinson's disease.

ER stress induces neuronal cell death in Alzheimer's and Parkinson's diseases [46, 47]. The ER stress response regulates neuronal apoptosis [48] via the activation of GADD153/CHOP, PERK, IRE1 α , eIF2 α and cleaved caspase-12 [49]. This process is suppressed by calbindins upregulation [19], whereas knockdown of calbindins increases cell death [50]. The induction of CaBP-28k expression occurs during the neuronal activation with elevated cytosolic calcium [51]. Furthermore, the intracellular calcium is significantly elevated in hippocampal neurons at old rats (12–16 months) compared with young rats (4–5 months), which means that neurons need a lot of calcium buffer function to comes with age [52]. We observed significantly higher expression of ER stress-related proteins in brains from old CaBP-9k KO mice, which were accompanied by increases in apoptosis-related proteins. We also found that the intracellular calcium is elevated in the CaBP-9k KO brain. Thus, CaBP-9k KO plays an important role in protecting the brain from ER stress-induced apoptosis and thus may represent a crucial target in treating neurodegenerative diseases.

Genetic mouse models of Alzheimer's and Parkinson's diseases exhibit pathological features and impaired memory and motor behaviors consistent with those observed in patients [53-56]. One study found that five gene mutations, including CaBP-28k KO, associated with familial Alzheimer's disease aggravate the disease pathogenesis at 6 months of age [57]. The number of CaBP-28k positive neurons was reduced in Alzheimer's disease, amyotrophic lateral sclerosis disease (ALS) and dementia patients [58, 59]. Other studies of CaBP-28k KO mice revealed signs of ataxia resulting from abnormal calcium transients in Purkinje dendrites [60, 61] and impaired fear memory and social behaviour as well as reduced anxiety-like behaviour in the elevated plus maze [62]. CaBP-28k expression has been shown to protect against pathological processes in Parkinson's disease [63, 64] and against the toxicity of 1-methyl-4-phenyl-1,2,3,6-tetrahydropyridine (MPTP) in dopaminergic cells [65]. Although the types of neurons expressing CaBP-9k and CaBP-28k are different, functions may be similar in the brain. Our results are similar to those of these studies, revealing abnormal memory and motor behaviors in CaBP-9k KO mice. We suggested that CaBP-9k also likely contributes to the pathogenesis of Alzheimer's and Parkinson's diseases.

TUDCA is a water-soluble bile acid, and it is the taurine conjugate of ursodeoxycholic acid [66, 67]. TUDCA reduces liver damage, oxidative stress, and scarring of tissue in mice [68]. TUDCA can cross the blood brain barrier [69], and alleviates some symptoms of neurodegenerative diseases. For example, TUDCA significantly reduces apoptosis caused by APP/ β -amyloid plaque accumulation in mouse brain [70] and rescues memory function in a mouse model of Alzheimer's disease [71]. TUDCA was also shown to prevent cell death in rodent models of Parkinson's disease [72-75]. Moreover, patients with amyotrophic lateral sclerosis that were treated with TUDCA had improved functional scores on measures of disability [76]. As TUDCA inhibits ER and oxidative stress [77, 78], we hypothesized that it would be beneficial in protecting the CaBP-9k KO mice from neurodegenerative disease-like pathology. Our results revealed that TUDCA reversed the alterations in memory and motor behaviors in CaBP-9k KO mice. These data suggest that pharmacological manipulation of ER stress or calcium homeostasis, such as with TUDCA, represents a potential intervention for symptoms of neurodegenerative disease.

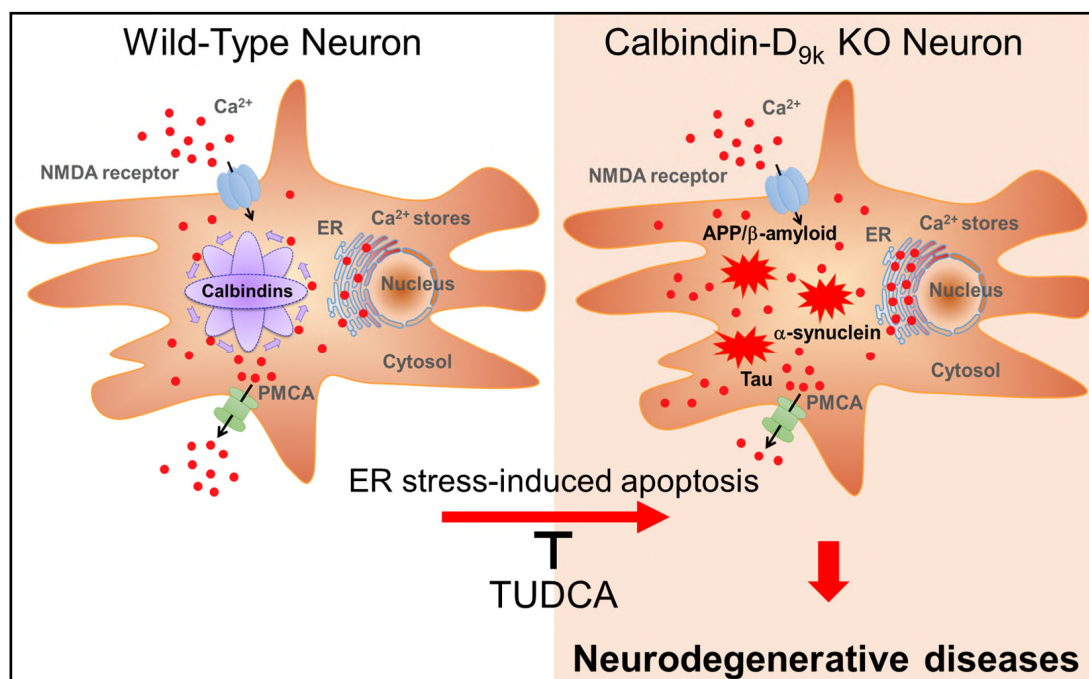


Fig. 8. Proposed model for neurodegenerative diseases. CaBP-9k KO brain has increased APP/ β -amyloid, Tau, and α -synuclein accumulation and endoplasmic reticulum (ER) stress-induced apoptosis. ER stress inhibitor TUDCA restored ER stress- and apoptosis-related gene expression to wild-type levels in CaBP-9k KO mice. Therefore, CaBP-9k may contribute to the onset and progression of neurodegenerative diseases.

Conclusion

This study is the first to demonstrate the role of CaBP-9k in the development of pathologies related to Alzheimer's and Parkinson's diseases. Of note, CaBP-9k represents critical regulators of calcium homeostasis, and the CaBP-9k KO mice described here represent a valuable animal model of neurodegenerative diseases. Furthermore, treatment with TUDCA can potentially prevent or slow neurodegenerative disease progression. Further research will focus on therapeutic strategies directly targeting drugs or hormones that regulate CaBP-9K expression (Fig. 8).

Abbreviations

CaBP-9k (calbindin-D_{9K}); CaBP-28k (calbindin-D_{28K}); ER (endoplasmic reticulum); APP (amyloid precursor protein); TUDCA (tauroursodeoxycholic acid); TH (tyrosine hydroxylase); BACE (beta-secretase); SNc (substantia nigra pars compacta); VTA (ventral tegmental area); Dat (dopamine active transporter); Ddc (dopadecarboxylase); Gfap (glial cell line-derived neurotrophic factor); ALS (amyotrophic lateral sclerosis disease); MPTP (1-methyl-4-phenyl-1,2,3,6-tetrahydropyridine).

Acknowledgements

Author contributions

E-M. J and E-B. J conceived the study, designed, performed and analyzed the experiments, and wrote the paper. S. P, B-H. J, C. A and Y-M. Y performed the experiments. E-J. H and W-Y. K revised the manuscript. E-B. J supervised the study.

Funding

This work was supported by the National Research Foundation of Korea (NRF) grant of Korean government (MEST) (2017R1A2B2005031) to E-B. J and Basic Science Research Program through the National Research Foundation of Korea (NRF) funded by the Ministry of Education (2018R1A6A3A11043046) to E-M. J. The funders had no role in study design, data collection and analysis, decision to publish, or preparation of the manuscript.

Disclosure Statement

The authors have no conflicts of interest to declare.

References

- 1 Bagur R, Hajnoczky G: Intracellular Ca²⁺ Sensing: Its Role in Calcium Homeostasis and Signaling. *Mol Cell* 2017;66:780-788.
- 2 Berridge MJ, Bootman MD, Roderick HL: Calcium signalling: dynamics, homeostasis and remodelling. *Nat Rev Mol Cell Biol* 2003;4:517-529.
- 3 LaFerla FM: Calcium dyshomeostasis and intracellular signalling in Alzheimer's disease. *Nat Rev Neurosci* 2002;3:862-872.
- 4 Chan CS, Gertler TS, Surmeier DJ: Calcium homeostasis, selective vulnerability and Parkinson's disease. *Trends Neurosci* 2009;32:249-256.
- 5 Maler L, Blankenship J, Rance M, Chazin WJ: Site-site communication in the EF-hand Ca²⁺-binding protein calbindin D9k. *Nat Struct Biol* 2000;7:245-250.

- 6 Gifford JL, Walsh MP, Vogel HJ: Structures and metal-ion-binding properties of the Ca²⁺-binding helix-loop-helix EF-hand motifs. *Biochem J* 2007;405:199-221.
- 7 Park SY, Yoo YM, Jung EM, Jeung EB: Distribution of and steroid hormone effects on calbindin-D9k in the immature rat brain. *Brain Res Bull* 2019;152:225-235.
- 8 Kim JH, Lee JA, Song YM, Park CH, Hwang SJ, Kim YS, Kaang BK, Son H: Overexpression of calbindin-D28K in hippocampal progenitor cells increases neuronal differentiation and neurite outgrowth. *FASEB J* 2006;20:109-111.
- 9 Odero GL, Oikawa K, Glazner KA, Schapansky J, Grossman D, Thiessen JD, Motnenko A, Ge N, Martin M, Glazner GW, Albensi BC: Evidence for the involvement of calbindin D28k in the presenilin 1 model of Alzheimer's disease. *Neuroscience* 2010;169:532-543.
- 10 Lazarov O, Peterson LD, Peterson DA, Sisodia SS: Expression of a familial Alzheimer's disease-linked presenilin-1 variant enhances perforant pathway lesion-induced neuronal loss in the entorhinal cortex. *J Neurosci* 2006;26:429-434.
- 11 McLachlan DR, Wong L, Bergeron C, Baimbridge KG: Calmodulin and calbindin D28K in Alzheimer disease. *Alzheimer Dis Assoc Disord* 1987;1:171-179.
- 12 Gerfen CR, Baimbridge KG, Miller JJ: The neostriatal mosaic: compartmental distribution of calcium-binding protein and parvalbumin in the basal ganglia of the rat and monkey. *Proc Natl Acad Sci U S A* 1985;82:8780-8784.
- 13 DiFiglia M, Christakos S, Aronin N: Ultrastructural localization of immunoreactive calbindin-D28k in the rat and monkey basal ganglia, including subcellular distribution with colloidal gold labeling. *J Comp Neurol* 1989;279:653-665.
- 14 Pan PY, Ryan TA: Calbindin controls release probability in ventral tegmental area dopamine neurons. *Nat Neurosci* 2012;15:813-815.
- 15 Voigtlander T, Unterberger U, Guentchev M, Schwaller B, Celio MR, Meyer M, Budka H: The role of parvalbumin and calbindin D28k in experimental scrapie. *Neuropathol Appl Neurobiol* 2008;34:435-445.
- 16 Yoo YM, Jeung EB: Calbindin-D28k in the Brain Influences the Expression of Cellular Prion Protein. *Oxid Med Cell Longev* 2018;2018:4670210.
- 17 Yoo YM, Jeung EB: Melatonin-induced estrogen receptor alpha-mediated calbindin-D9k expression plays a role in H2O2-mediated cell death in rat pituitary GH3 cells. *J Pineal Res* 2009;47:301-307.
- 18 Yoo YM, Jeung EB: Melatonin-induced calbindin-D9k expression reduces hydrogen peroxide-mediated cell death in rat pituitary GH3 cells. *J Pineal Res* 2010;48:83-93.
- 19 Jung EM, An BS, Choi KC, Jeung EB: Apoptosis- and endoplasmic reticulum stress-related genes were regulated by estrogen and progesterone in the uteri of calbindin-D(9k) and -D(28k) knockout mice. *J Cell Biochem* 2012;113:194-203.
- 20 Lee GS, Lee KY, Choi KC, Ryu YH, Paik SG, Oh GT, Jeung EB: Phenotype of a calbindin-D9k gene knockout is compensated for by the induction of other calcium transporter genes in a mouse model. *J Bone Miner Res* 2007;22:1968-1978.
- 21 Jung EM, Moffat JJ, Liu J, Dravid SM, Gurumurthy CB, Kim WY: Arid1b haploinsufficiency disrupts cortical interneuron development and mouse behavior. *Nat Neurosci* 2017;20:1694-1707.
- 22 Jung EM, Ka M, Kim WY: Loss of GSK-3 Causes Abnormal Astrogenesis and Behavior in Mice. *Mol Neurobiol* 2016;53:3954-3966.
- 23 Wang CY, Liao JK: A mouse model of diet-induced obesity and insulin resistance. *Methods Mol Biol* 2012;821:421-433.
- 24 Festing MF, Altman DG: Guidelines for the design and statistical analysis of experiments using laboratory animals. *ILAR J* 2002;43:244-258.
- 25 O'Brien RJ, Wong PC: Amyloid precursor protein processing and Alzheimer's disease. *Annu Rev Neurosci* 2011;34:185-204.
- 26 Jones R: Neurological disorders: Two sides to beta-amyloid. *Nat Rev Neurosci* 2012;13:666.
- 27 Congdon EE, Sigurdsson EM: Tau-targeting therapies for Alzheimer disease. *Nat Rev Neurol* 2018;14:399-415.
- 28 He Z, Guo JL, McBride JD, Narasimhan S, Kim H, Changolkar L, Zhang B, Gathagan RJ, Yue C, Dengler C, Stieber A, Nitla M, Coulter DA, Abel T, Brunden KR, Trojanowski JQ, Lee VM: Amyloid-beta plaques enhance Alzheimer's brain tau-seeded pathologies by facilitating neuritic plaque tau aggregation. *Nat Med* 2018;24:29-38.

- 29 Suh YH, Checler F: Amyloid precursor protein, presenilins, and alpha-synuclein: molecular pathogenesis and pharmacological applications in Alzheimer's disease. *Pharmacol Rev* 2002;54:469-525.
- 30 Poewe W, Seppi K, Tanner CM, Halliday GM, Brundin P, Volkman J, Schrag AE, Lang AE: Parkinson disease. *Nat Rev Dis Primers* 2017;3:17013.
- 31 Lotharius J, Brundin P: Pathogenesis of Parkinson's disease: dopamine, vesicles and alpha-synuclein. *Nat Rev Neurosci* 2002;3:932-942.
- 32 Schwaller B: Cytosolic Ca²⁺ buffers. *Cold Spring Harb Perspect Biol* 2010;2:a004051.
- 33 Phillips W, Michell A, Pruess H, Barker RA: Animal models of neurodegenerative diseases. *Methods Mol Biol* 2009;549:137-155.
- 34 Xie Q, Khaoustov VI, Chung CC, Sohn J, Krishnan B, Lewis DE, Yoffe B: Effect of tauroursodeoxycholic acid on endoplasmic reticulum stress-induced caspase-12 activation. *Hepatology* 2002;36:592-601.
- 35 Hennings H, Michael D, Cheng C, Steinert P, Holbrook K, Yuspa SH: Calcium regulation of growth and differentiation of mouse epidermal cells in culture. *Cell* 1980;19:245-254.
- 36 Berridge MJ: Calcium signalling and cell proliferation. *Bioessays* 1995;17:491-500.
- 37 Pinton P, Giorgi C, Siviero R, Zecchini E, Rizzuto R: Calcium and apoptosis: ER-mitochondria Ca²⁺ transfer in the control of apoptosis. *Oncogene* 2008;27:6407-6418.
- 38 Brini M, Cali T, Ottolini D, Carafoli E: Neuronal calcium signaling: function and dysfunction. *Cell Mol Life Sci* 2014;71:2787-2814.
- 39 Kennedy MB: Regulation of neuronal function by calcium. *Trends Neurosci* 1989;12:417-420.
- 40 Simons TJ: Calcium and neuronal function. *Neurosurg Rev* 1988;11:119-129.
- 41 Denessiouk K, Permyakov S, Denesyuk A, Permyakov E, Johnson MS: Two structural motifs within canonical EF-hand calcium-binding domains identify five different classes of calcium buffers and sensors. *PLoS One* 2014;9:e109287.
- 42 Clapham DE: Calcium signaling. *Cell* 2007;131:1047-1058.
- 43 Choi KC, Jeung EB: Molecular mechanism of regulation of the calcium-binding protein calbindin-D9k, and its physiological role(s) in mammals: a review of current research. *J Cell Mol Med* 2008;12:409-420.
- 44 Sloviter RS: Calcium-binding protein (calbindin-D28k) and parvalbumin immunocytochemistry: localization in the rat hippocampus with specific reference to the selective vulnerability of hippocampal neurons to seizure activity. *J Comp Neurol* 1989;280:183-196.
- 45 He H, Lam M, McCormick TS, Distelhorst CW: Maintenance of calcium homeostasis in the endoplasmic reticulum by Bcl-2. *J Cell Biol* 1997;138:1219-1228.
- 46 Salminen A, Kauppinen A, Suuronen T, Kaarniranta K, Ojala J: ER stress in Alzheimer's disease: a novel neuronal trigger for inflammation and Alzheimer's pathology. *J Neuroinflammation* 2009;6:41.
- 47 Wu L, Tian YY, Shi JP, Xie W, Shi JQ, Lu J, Zhang YD: Inhibition of endoplasmic reticulum stress is involved in the neuroprotective effects of candesartan cilexetil in the rotenone rat model of Parkinson's disease. *Neurosci Lett* 2013;548:50-55.
- 48 Sano R, Reed JC: ER stress-induced cell death mechanisms. *Biochim Biophys Acta* 2013;1833:3460-3470.
- 49 Iurlaro R, Munoz-Pinedo C: Cell death induced by endoplasmic reticulum stress. *FEBS J* 2016;283:2640-2652.
- 50 Jung EM, Choi KC, Jeung EB: Expression of calbindin-D28k is inversely correlated with proapoptotic gene expression in hydrogen peroxide-induced cell death in endometrial cancer cells. *Int J Oncol* 2011;38:1059-1066.
- 51 Lowenstein DH, Miles MF, Hatam F, McCabe T: Up regulation of calbindin-D28K mRNA in the rat hippocampus following focal stimulation of the perforant path. *Neuron* 1991;6:627-633.
- 52 Raza M, Deshpande LS, Blair RE, Carter DS, Sombati S, DeLorenzo RJ: Aging is associated with elevated intracellular calcium levels and altered calcium homeostatic mechanisms in hippocampal neurons. *Neurosci Lett* 2007;418:77-81.
- 53 Gotz J, Ittner LM: Animal models of Alzheimer's disease and frontotemporal dementia. *Nat Rev Neurosci* 2008;9:532-544.
- 54 Kobayashi DT, Chen KS: Behavioral phenotypes of amyloid-based genetically modified mouse models of Alzheimer's disease. *Genes Brain Behav* 2005;4:173-196.
- 55 Dawson TM, Ko HS, Dawson VL: Genetic animal models of Parkinson's disease. *Neuron* 2010;66:646-661.
- 56 Jagmag SA, Tripathi N, Shukla SD, Maiti S, Khurana S: Evaluation of Models of Parkinson's Disease. *Front Neurosci* 2015;9:503.

- 57 Kook SY, Jeong H, Kang MJ, Park R, Shin HJ, Han SH, Son SM, Song H, Baik SH, Moon M, Yi EC, Hwang D, Mook-Jung I: Crucial role of calbindin-D28k in the pathogenesis of Alzheimer's disease mouse model. *Cell Death Differ* 2014;21:1575-1587.
- 58 Lally G, Faull RL, Waldvogel HJ, Ferrari S, Emson PC: Calcium homeostasis in ageing: studies on the calcium binding protein calbindin D28K. *J Neural Transm (Vienna)* 1997;104:1107-1112.
- 59 Ferrer I, Tunon T, Serrano MT, Casas R, Alcantara S, Zujar MJ, Rivera RM: Calbindin D-28k and parvalbumin immunoreactivity in the frontal cortex in patients with frontal lobe dementia of non-Alzheimer type associated with amyotrophic lateral sclerosis. *J Neurol Neurosurg Psychiatry* 1993;56:257-261.
- 60 Airaksinen MS, Eilers J, Garaschuk O, Thoenen H, Konnerth A, Meyer M: Ataxia and altered dendritic calcium signaling in mice carrying a targeted null mutation of the calbindin D28k gene. *Proc Natl Acad Sci U S A* 1997;94:1488-1493.
- 61 Barski JJ, Hartmann J, Rose CR, Hoebeek F, Morl K, Noll-Hussong M, De Zeeuw CI, Konnerth A, Meyer M: Calbindin in cerebellar Purkinje cells is a critical determinant of the precision of motor coordination. *J Neurosci* 2003;23:3469-3477.
- 62 Harris EP, Abel JM, Tejada LD, Rissman EF: Calbindin Knockout Alters Sex-Specific Regulation of Behavior and Gene Expression in Amygdala and Prefrontal Cortex. *Endocrinology* 2016;157:1967-1979.
- 63 Yamada T, McGeer PL, Baimbridge KG, McGeer EG: Relative sparing in Parkinson's disease of substantia nigra dopamine neurons containing calbindin-D28K. *Brain Res* 1990;526:303-307.
- 64 Wang C, Jiang C, Yuan H, Xiao C, Gao D: Role of calbindin-D28K in estrogen treatment for Parkinson's disease. *Neural Regen Res* 2013;8:702-707.
- 65 Yuan HH, Chen RJ, Zhu YH, Peng CL, Zhu XR: The neuroprotective effect of overexpression of calbindin-D(28k) in an animal model of Parkinson's disease. *Mol Neurobiol* 2013;47:117-122.
- 66 Neuman MG, Cameron RG, Shear NH, Bellentani S, Tiribelli C: Effect of tauroursodeoxycholic and ursodeoxycholic acid on ethanol-induced cell injuries in the human Hep G2 cell line. *Gastroenterology* 1995;109:555-563.
- 67 Vang S, Longley K, Steer CJ, Low WC: The Unexpected Uses of Urso- and Tauroursodeoxycholic Acid in the Treatment of Non-liver Diseases. *Glob Adv Health Med* 2014;3:58-69.
- 68 Cho EJ, Yoon JH, Kwak MS, Jang ES, Lee JH, Yu SJ, Kim YJ, Kim CY, Lee HS: Tauroursodeoxycholic acid attenuates progression of steatohepatitis in mice fed a methionine-choline-deficient diet. *Dig Dis Sci* 2014;59:1461-1474.
- 69 Parry GJ, Rodrigues CM, Aranha MM, Hilbert SJ, Davey C, Kelkar P, Low WC, Steer CJ: Safety, tolerability, and cerebrospinal fluid penetration of ursodeoxycholic Acid in patients with amyotrophic lateral sclerosis. *Clin Neuropharmacol* 2010;33:17-21.
- 70 Sola S, Amaral JD, Borralho PM, Ramalho RM, Castro RE, Aranha MM, Steer CJ, Rodrigues CM: Functional modulation of nuclear steroid receptors by tauroursodeoxycholic acid reduces amyloid beta-peptide-induced apoptosis. *Mol Endocrinol* 2006;20:2292-2303.
- 71 Lo AC, Callaerts-Vegh Z, Nunes AF, Rodrigues CM, D'Hooge R: Tauroursodeoxycholic acid (TUDCA) supplementation prevents cognitive impairment and amyloid deposition in APP/PS1 mice. *Neurobiol Dis* 2013;50:21-29.
- 72 Castro-Caldas M, Carvalho AN, Rodrigues E, Henderson CJ, Wolf CR, Rodrigues CM, Gama MJ: Tauroursodeoxycholic acid prevents MPTP-induced dopaminergic cell death in a mouse model of Parkinson's disease. *Mol Neurobiol* 2012;46:475-486.
- 73 Duan WM, Rodrigues CM, Zhao LR, Steer CJ, Low WC: Tauroursodeoxycholic acid improves the survival and function of nigral transplants in a rat model of Parkinson's disease. *Cell Transplant* 2002;11:195-205.
- 74 Keene CD, Rodrigues CM, Eich T, Linehan-Stieers C, Abt A, Kren BT, Steer CJ, Low WC: A bile acid protects against motor and cognitive deficits and reduces striatal degeneration in the 3-nitropropionic acid model of Huntington's disease. *Exp Neurol* 2001;171:351-360.
- 75 Keene CD, Rodrigues CM, Eich T, Chhabra MS, Steer CJ, Low WC: Tauroursodeoxycholic acid, a bile acid, is neuroprotective in a transgenic animal model of Huntington's disease. *Proc Natl Acad Sci U S A* 2002;99:10671-10676.
- 76 Elia AE, Lalli S, Monsurro MR, Sagnelli A, Taiello AC, Reggiori B, La Bella V, Tedeschi G, Albanese A: Tauroursodeoxycholic acid in the treatment of patients with amyotrophic lateral sclerosis. *Eur J Neurol* 2016;23:45-52.

- 77 Yoon YM, Lee JH, Yun SP, Han YS, Yun CW, Lee HJ, Noh H, Lee SJ, Han HJ, Lee SH: Tauroursodeoxycholic acid reduces ER stress by regulating of Akt-dependent cellular prion protein. *Sci Rep* 2016;6:39838.
- 78 Ozcan U, Yilmaz E, Ozcan L, Furuhashi M, Vaillancourt E, Smith RO, Gorgun CZ, Hotamisligil GS: Chemical chaperones reduce ER stress and restore glucose homeostasis in a mouse model of type 2 diabetes. *Science* 2006;313:1137-1140.